Applied Catalysis B: Environmental 108–109 (2011) 61–71

Contents lists available at ScienceDirect

Applied Catalysis B: Environmental

journal homepage: www.elsevier.com/locate/apcatb

Liquid-phase degradation of polyethylene (PE) over MFI zeolites with mesopores: Effects of the structure of PE and the characteristics of mesopores

Jae Youl Lee, Se Min Park, Shyamal Kumar Saha [1], Sung June Cho, Gon Seo *

School of Applied Chemical Engineering, Chonnam National University, Gwangju 500-757, Republic of Korea

ARTICLE INFO

Article history:
Received 9 May 2011
Received in revised form 23 July 2011
Accepted 10 August 2011
Available online 22 August 2011

Keywords:
Degradation
Polyethylene
MFI zeolite
Mesopore
Acidity

ABSTRACT

Four kinds of MFI-meso zeolites with both micro- and mesopores were prepared, characterized, and their catalytic activities were evaluated in the liquid-phase degradation of high-density, low-density, and linear low-density polyethylene (HDPE, LDPE, and LLDPE) in order to discuss their catalytic performance in relation to their porous characteristics and acidity. MFI-syn that was synthesized from partially dissolved MFI zeolite and MFI-sda that was prepared by using a special structure directing agent exhibited highly ordered mesopores with strong acidity and achieved high conversions, about 95%, even with small catalyst loadings (HDPE/catalyst = 20 g/0.05 g) at 380 °C. However, MFI-oxy prepared from an oxyacid-added mixture exhibited a poor catalytic activity because of its low acidity and small pore volume. MFI-alk prepared by an alkali treatment exhibited irregular mesopores and medium conversions. MFI-meso zeolites were especially suitable for the degradation of HDPE and LLDPE, which required a high external surface for the initial degradation of polyethylene and a rapid mass transfer, resulting in a higher catalytic activity. The enhancement of catalytic activity in the degradation of LDPE by the introduction of mesopores was relatively small because of its rapid initial degradation.

1. Introduction

The production amounts of polyolefins, such as polyethylene (PE) and polypropylene (PP), have been steadily increasing because of their low cost and high convenience, but their short life times causes rapid increases in their disposal amounts. Although the material recycling of separately collected PE and PP is very effective in minimizing their disposal, the poor properties and low value of recycled products limit the recycled amount [1]. Landfill and incineration are easily utilized for disposal, but these disposal methods are banned because contamination of soil and air is inevitable [1,2]. However, the degradation of polyolefins produces gas and liquid fuels composed of lower hydrocarbons. The degradation occurs at higher temperatures, but a huge amount of energy for heating and a wide distribution of product compositions reduce the feasibility of thermal degradation. Catalytic degradation at lower temperatures with a small amount of energy, therefore, economically facilitates the conversion of waste PE and PP into fuels with relatively narrow product compositions ($<C_{12}$) that are convenient for use [2].

Zeolites with high surface areas and strong acidity have been extensively applied as catalysts in the degradation of PE [1–7]. Since large polymer molecules cannot intrude into the micropores of zeolites, the initial degradation on the external surface is essential and further degradation at the entrances and pores of zeolites produces low molecular weight hydrocarbons. Therefore, the area of the external surface, pore structure, and acidity of zeolite largely affect their catalytic activity with respect to the degradation of PE [8]. Nano size MFI and BEA zeolites with bent pores suppressing the formation of large hydrocarbon molecules, the precursors of coke deposits, are considered to be promising catalysts, but small zeolite particles are difficult to handle, limiting their use as catalysts for degradation [9–14].

The presence of mesopores in MFI zeolite enlarges the surface area and divides it into small zeolite moieties to achieve good contact with large polymer molecules, and this reduces the diffusion length in particles, like nano-sized zeolites, involved in catalytic reactions with diffusion limitations [15–19]. Several methods for the introduction of mesopores into MFI zeolites have been reported in the literature [20–27]. The partial dissolution of the zeolite framework by alkali produces mesopores in zeolite crystals [20–22]. The crystallization of mesoporous material from a synthetic mixture containing dissolved MFI zeolite also facilitates the preparation of zeolites with both micro- and mesopores [23]. The use of a special structure directing agent (sda) for the concomitant formation of mesopores with MFI zeolite and the addition of oxyacids into the synthetic mixture of MFI zeolite are very effective in the synthesis of MFI zeolite with mesopores in a very short time [24,25]. The crystallization of MFI zeolite from the synthetic

* Corresponding author. Tel.: +82 62 530 1876; fax: +82 62 530 1899.
E-mail address: gseo@chonnam.ac.kr (G. Seo).
[1] Present address: The Energy Institute, Pennsylvania State University, 209 Academic Projects Bld., University Park, PA 16802, USA.

0926-3373/$ – see front matter © 2011 Elsevier B.V. All rights reserved.
doi:10.1016/j.apcatb.2011.08.009

mixture containing nano-size organic materials, such as carbon black, polystyrene, etc., which can be easily removed by calcination, also achieves both micro- and mesopores [22,26]. The formation of mesopores accompanying the zeolitic micropores can be confirmed from their adsorption isotherms of nitrogen, but the confirmation of mesopores with a surface consisting of MFI zeolite is not easy.

The presence of mesopores on MFI zeolite enhances the catalytic activity by enlarging its external surface for the initial degradation of large polymer molecules. However, the contribution of mesopores on the catalytic degradation of PEs strongly depends on their skeletal structure. The introduction of mesopores on MFI zeolite considerably improves the degradation of HDPE by providing a large external surface because its initial degradation on acid sites is slow. On the contrary, the improvement of LDPE degradation by the introduction of mesopores is not significant compared to that of HDPE degradation because the long branched hydrocarbons of LDPE easily form tertiary carbenium ions on acid sites [27]. The diffusion of degraded products in mesopores also improves the catalytic degradation, but the extent of improvement is largely dependent on the characteristics of mesopores and the skeletal structure of PEs [28–30].

Several evaluation methods for the catalytic activity of solid acids in the degradation of PEs have been used. The activation energy and rate constant deduced from the kinetic data of thermogravimetric experiments are suitable for the quantitative comparison of catalytic activities [27,31]. The initiation and completion temperatures for the degradation are also useful. The minimum amount of catalysts required for the complete degradation of PE at a given temperature provides a good evaluation scale [9]. Although kinetic parameters are adequate for the deduction of intrinsic catalytic activities, the required amounts of catalysts for a complete degradation are more effective in industrial aspects because the degradation of PE is carried out through multi-step reactions in heterogeneous states. The nonuniform dispersion of solid catalysts in molten PE and their deactivation by coke deposits inevitably induce large variations in their activities.

In this study, we prepared four kinds of MFI zeolites with mesopores (abbreviated hereafter MFI-meso zeolites) by treatment with an alkaline solution, the addition of a special sda and an oxyacid, and the synthesis of a mesoporous material from a synthetic mixture containing dissolved MFI fragments. TEM, argon adsorption–desorption isotherms, temperature-programmed desorption (TPD) profiles of ammonia, and the uptake of *o*-xylene were used to characterize the porous and acidic properties of the MFI-meso zeolites. The presence of the MFI framework on the mesopores is, firstly, to our knowledge, confirmed using the analysis of TEM images. Their catalytic activities in the liquid-phase degradation of PEs with different skeletal structures, such as HDPE, LDPE, and LLDPE, were discussed in relation to the types of mesopores and acidity. Since the molecular weights of PEs influence their degradation reactivity in terms of fluidity and diffusivity, PEs with similar number average molecular weights were used as reactants.

2. Experimental

2.1. Preparation of MFI zeolites with mesopores

MFI-meso zeolites with mesopores were prepared with four methods and were denoted as MFI-x, where x represented the preparation method. MFI-syn was synthesized from the synthetic mixture containing fragments of commercial MFI zeolite (CBV 5522G, Zeolyst Co.) dissolved in 0.2 N NaOH (99.9%, Daejung) solution and *n*-hexadecyltrimethyl ammonium bromide (HDAB, 98%, Alfaaesra) as a sda for mesopores. After mixing for 1 h, the synthetic mixture was heated at 97 °C for 5 days for a hydrothermal reaction. The pH of the mixture was adjusted to 11 after each 24 h reaction by acetic acid (99%, Daejung) [23]. The solid phase was washed with deionized water and dried at 100 °C and the template that was occluded in the mesopores was removed by calcination at 550 °C for 8 h. Cations of MFI-syn were exchanged with ammonium ions with 0.5 N ammonium nitrate (98% Daejung) at 60 °C for 24 h and its H-form was obtained by calcination at 550 °C for 8 h.

MFI-sda was synthesized using a special sda, octadecyldimethyl 3-trimethoxysilylpropyl ammonium chloride (60% in methanol, OTAC, Abcr) [24]. Tetraethyl orthosilicate (TEOS, 98%, Aldrich), sodium aluminate (31% Na_2O, 34% Al_2O_3, Kanto), and tetrapropylammonium bromide (TPABr, 98%, Acros) were also used for the preparation of the synthetic mixture with its composition of 38 SiO_2:1 Al_2O_3:10 TPABr:10 Na_2O:2 OTAC:7200 H_2O. After mixing at ambient temperature for 2 h, the synthetic mixture was heated at 130 °C for 5 days in an autoclave. The rest of the preparation procedure for H-form MFI-sda was the same as that of the procedure described above.

MFI-alk was prepared by treating the commercial MFI zeolite with 0.2 N NaOH solution at 80 °C for 5 h. After washing with deionized water, the solid that remained was collected by centrifuging and H-form MFI-syn was obtained following the procedure described above.

MFI-oxy was synthesized by the addition of perchloric acid (60%, Aldrich) to a synthetic mixture for MFI zeolite [25]. The composition of the synthetic mixture prepared using tetrapropyl ammonium hydroxide (TPAOH, 98%, Aldrich), sodium aluminate, and TEOS was 1 TEOS:0.025 Al_2O_3:0.4 TPAOH:0.1 $HClO_4$:25 H_2O and the synthetic mixture was hydrothermally reacted at 140 °C for 6 h in an autoclave. Washing, drying, calcining, and ion exchanging for the preparation of H-form MFI-oxy was the same as the procedure described above.

The commercial MFI zeolite (MFI-nano) with 200–500 nm crystallites and a MFI zeolite composed of large crystalline plates (MFI-plate) that were synthesized by the conventional method were used as reference MFI zeolites for comparison [32].

2.2. Characterization of MFI-meso zeolites

X-ray diffraction (XRD) patterns of the MFI zeolites were recorded on a high resolution X-ray diffractometer (Rigaku D/Max Ultima III) at 40 kV and 40 mA with CuKα radiation (λ = 1.54056 Å) filtered by a Ni-filter. Their shape and size were examined using a SEM (JEOL, JSM-5400). The dissolved solutions of the MFI zeolites in HF were analyzed by using an induced coupled plasma spectrometer (ICP, Perkin Elmer, OPTIMA 4300 DV) to determine their Si/Al molar ratios. Their compositions were also confirmed by an energy dispersed X-ray analysis (EDX) with an EDX system equipped on a SEM (Hitachi, S-4700). TEM examination was performed using Tecnai F20 (Philips) at an accelerating voltage of 200 kV. The samples were prepared by dropping ethanol suspensions of fine powders onto a holey carbon grid and subsequently subjected to drying. The TEM image was analyzed using the Electron Direct Methods (EDM) program package [33] and Visual Computing in Electron Crystallography [34].

MAS NMR spectra of ^{27}Al in the MFI zeolites were obtained using a 200 MHz superconducting solid FT-NMR spectrometer (Varian, Unity Solid Inova WB 200 MHz system) at a rotating speed of 5 kHz. A microwave of 39.793 kHz corresponding to the ^{27}Al species irradiated the zeolite samples with 90° pulses that were 5 μs long. The repeating time for pulses was 1 s and 2000 scans were accumulated to enhance the signal-to-noise ratio.

Adsorption isotherms of argon on the MFI zeolites were obtained using a surface area analyzer (Micrometrics, ASAP 2000). The samples were evacuated at 300 °C for 15 h prior

to exposure to argon gas (99.9999%, DongA) at liquid argon temperature (−186 °C). The surface area was calculated using the Brunaure–Emmett–Teller (BET) equation. The size distributions of micropores and mesopores were obtained using the Horvath–Kawazoe equation and the Barett, Joyner, and Halender (BJH) method, respectively.

Uptake curves of *o*-xylene on the MFI zeolites were measured using a home-made gravimetric adsorption system equipped with a quartz spring [10]. A sample of 0.1 g charged in a quartz basket was evacuated at 300 °C for 2 h. After cooling to 120 °C, *o*-xylene (99%, Yakuri) vapor was supplied to the sample. The increase of the mass with the adsorption was continuously recorded for 60 min.

TPD profiles of ammonia from the MFI zeolites were obtained using a home-made TPD apparatus [9]. A sample of 0.1 g was activated at 550 °C for 2 h in a helium (99.999%, DongA) flow of 100 ml/min and cooled to 150 °C. The sample was exposed to ammonia (99.999%, Daehan Standard Gas) pulses until the sample was saturated with ammonia. Physically adsorbed ammonia was removed by purging the helium flow at the same temperature. The temperature of the sample increased to 600 °C with a ramping rate of 10 °C/min and the amount of ammonia desorbed from the sample was continuously monitored by a mass spectrometer (Balzers, TCP 015). The amount of strong acid sites of MFI zeolites were calculated from the deconvoluted TPD profiles and represented with a relative amount of strong acid sites to that of the MFI-plate with the largest amount of strong acid sites.

2.3. Liquid-phase degradation of PEs

Three PEs with different skeletal structures, such as HDPE, LDPE, and LLDPE, were used as reactants for liquid-phase catalytic degradation. Their physical properties that were provided by manufactures are summarized below: HDPE had a high molecular weight, and thereby had a low melt index and high T_m. The molecular weight of LLDPE was slightly higher than that of LDPE, but the former had a relatively high melt index compared to the latter due to the former's linear skeletal structure.

Polymer	Molecular weight		Melt index (g/10 min)	Density (g/cm^3)	T_m (°C)	Manufacture (Grade)
	Number-average	Weight-average				
HDPE	41,100	279,900	0.35	0.965	134	Honam Petrochemical Corp. (5200B)
LDPE	20,700	129,900	1.00	0.923	113	LG Chem. (BF315)
LLDPE	34,100	137,400	1.30	0.920	120	LG Chem. (SF315)

The liquid-phase degradation of PEs on zeolites was carried out in a batch reactor described in our previous paper [9]. Typically, a mixture of HDPE and zeolite was charged into a 100 ml round-bottomed flask and purged with N_2 flow at 45 cm^3/min to remove oxygen. Since the thermal degradation of PEs occurred above 400 °C, the reaction temperature was fixed to 380 °C to minimize their thermal degradation.

The conversion was defined as the percentage of PEs converted to gas and liquid products [9]. The conversions were determined by adding the yields of liquid and gas products during the degradation and the conversions at the final reaction time were confirmed by the changes in the weights of the round-bottomed flask before and after the degradation. The yields of the liquid products were determined from the amount of liquid collected in the burette and the yields of the gas products were obtained from the difference between the conversion and the yield of liquid products. The yield of gas products was also confirmed by the amount of gas products accumulated in the degradation under an assumption that the gas products were equimolar mixtures of propylene and butene.

3. Results and discussion

3.1. Characterization of mesopores on MFI-meso zeolites

XRD patterns of the MFI-meso zeolites should be different from those of MFI zeolites and mesoporous materials, because they have characteristics of both zeolite and mesoporous materials. Fig. 1 shows the XRD patterns of four MFI zeolites and two reference MFI zeolites. MFI-syn and MFI-sda had high peaks at $2\theta = 2.0°$, which were attributed to mesopores accompanying small peaks at $2\theta = 8–10°$ and $2\theta = 24–28°$ that were attributed to the MFI framework, indicating the co-presence of mesopores with diameters of around 30 Å and an MFI framework [24]. However, the lack of diffraction peaks attributed to the mesopores and the low diffraction peaks attributed to the MFI framework of MFI-alk and MFI-oxy reflected the low regularity of the mesopores. In addition, the small zeolite moieties of the MFI-meso zeolites caused lower diffraction peaks.

Fig. 2 shows SEM photos of four MFI-meso zeolites and two reference MFI zeolites. Although particle shapes and sizes varied with their preparation methods, the particle sizes of the MFI-meso zeolites were commonly less than 1 μm. Otherwise, the MFI-plate was composed of larger hexagonal plates that were 0.5 μm × 2 μm and the MFI-nano of round particles that were less than 500 nm.

The co-presence of mesopores and micropores in the MFI-meso zeolites could be confirmed by their adsorption isotherms, as shown in Fig. S1. The four MFI-meso zeolites exhibited common hysteresis loops on their argon adsorption–desorption isotherms, clearly indicating the presence of mesopores. The steep increases in the adsorption amount at $P/P_0 \rightarrow 0$ were responsible for the micropores of the zeolite framework. The variance in the shape and size of the hysteresis loops according to preparation method suggested that the shapes of mesopores formed on the MFI-meso zeolites varied. The MFI-nano exhibited a gradual increase in the amount of argon adsorbed on it with increasing pressure, revealing the presence of mesopores formed among small nano size particles. On the contrary, a typical Langmuir type isotherm of the MFI-plate indicated only the presence of micropores.

Fig. 3 shows the size distributions of micropores and mesopores on the MFI-meso and reference MFI zeolites. All the zeolites, regardless of the presence of mesopores, consistently exhibited a peak at $D = 0.5$ nm, confirming the presence of zeolite micropores [22]. Another peak at around 0.7 nm was observed for the MFI-oxy, MFI-nano, and MFI-plate, indicating the presence of slightly large micropores. Even the MFI-plate with definite crystals also had the same pores, and thereby the pores should be related to the pores of MFI zeolites themselves. The cross sections of two channels might cause such large pores, but more work is required to verify them. The relatively small micropore volumes of MFI-syn and MFI-sda correspond to the small amount of MFI zeolite moiety on them, because only their mesopore walls were composed of MFI zeolite. However, MFI-alk and MFI-oxy had relatively large volumes of micropores because bulk zeolite was present on them.

The size of mesopores on the MFI-meso zeolites also varied with their preparation method. MFI-syn and MFI-sda with their large mesopore volumes also had wide ranges of mesopore diameters. On the contrary, the mesopores of MFI-alk and MFI-oxy possessed

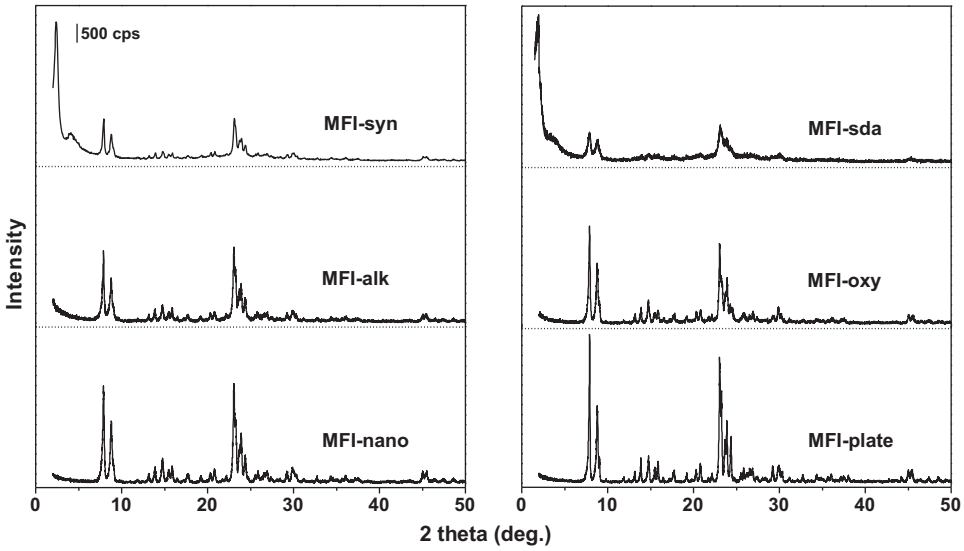

Fig. 1. X-ray diffraction patterns of MFI zeolites.

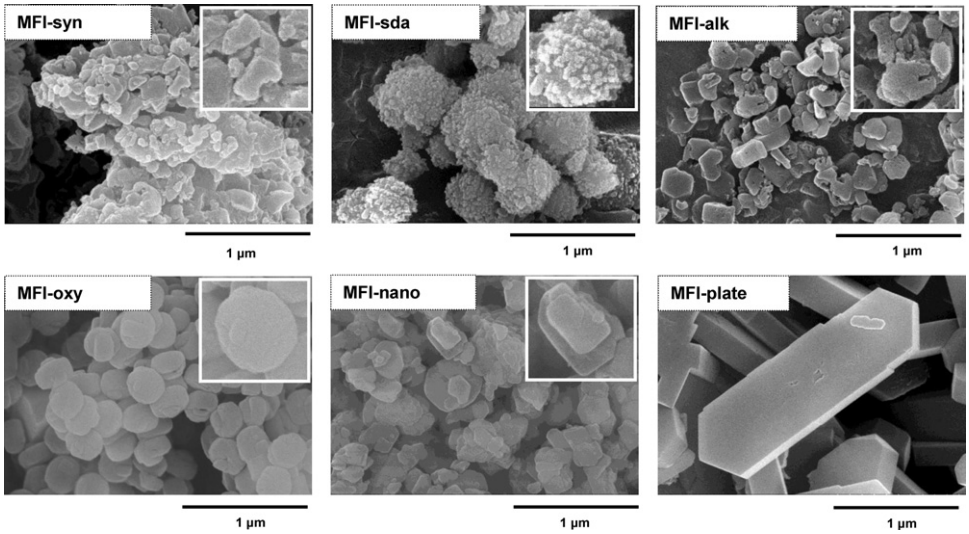

Fig. 2. SEM photos of MFI zeolites.

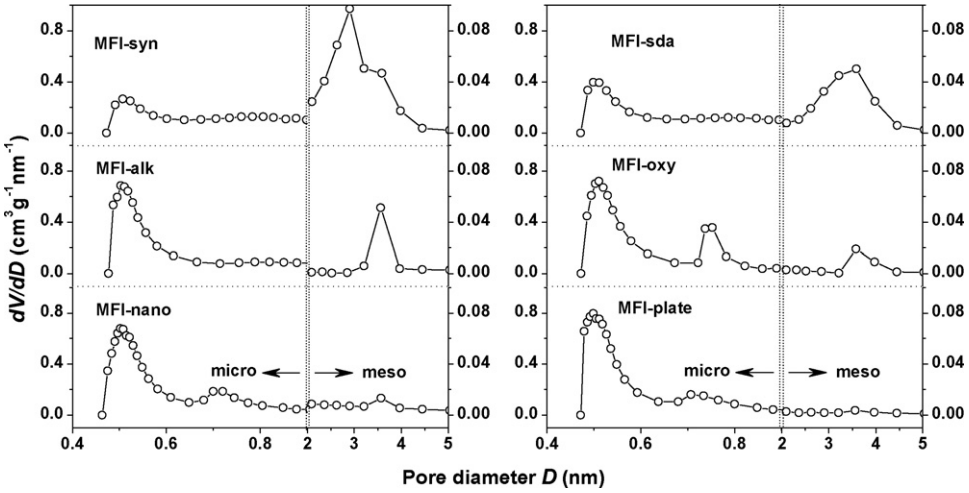

Fig. 3. Size distributions of micropores and mesopores on MFI zeolites.

relatively narrow ranges of diameters at around $D = 3.5$ nm. The amount of mesopores on MFI-oxy was very small compared to those of other MFI-meso zeolites. Unexpectedly, MFI-nano had a trace peak, which indicated the presence of a very small amount of mesopores due to voids formed among the nano sized particles.

Table 1 lists the Si/Al molar ratios, pore volumes, BET surface areas, particle sizes, and relative amounts of strong acid sites of the MFI-meso zeolites. The Si/Al ratios measured using ICP and EDX methods exhibited good agreement between them. MFI-sda, MFI-alk, and MFI-oxy had low Si/Al ratios, suggesting their high acid site density, while the MFI-syn and MFI-nano had high Si/Al ratios. The amounts of micropores and mesopores increased together in the order of MFI-oxy < -alk < -sda < -syn. MFI-syn had the largest volumes of micro- and mesopores, and thus its total pore volume reached 0.8 cm^3/g. On the contrary, MFI-oxy had small amounts of micropores and mesopores (0.11 and 0.13 cm^3/g, respectively). MFI-plate with large particles had a negligible amount of mesopores. The BET surface areas of the MFI-meso zeolites increased in the same order of total pore volume: MFI-syn with the largest pore volume resulted in the highest BET surface area, while MFI-oxy with the smallest pore volume resulted in the lowest BET surface area. Although the surface area of the MFI zeolite was usually dependent on the micropore volume, the mesopore volumes of the MFI-meso zeolites played an important role in determining their surface areas.

The TEM images shown in Fig. 4 also confirmed the presence of mesopores on the MFI-meso zeolites. MFI-syn and MFI-sda exhibited uniformly developed mesopore lattices due to the arrayed HDAB and OTAC micelles. However, many spherical voids with different sizes were observed on MFI-alk prepared by the alkali treatment. The zeolite moiety that was dissolved with alkali produced heterogeneous mesopores. MFI-oxy exhibited large voids. The aggregated oxyacid molecules that were added in the synthetic mixture occupied large volumes and their removal left large voids. The regularly ordered mesopores of MFI-syn and MFI-syn caused clear diffraction peaks attributed to mesopores on their XRD patterns (Fig. 1). On the contrary, the heterogeneity in the size and arrangement of mesopores on the MFI-alk and MFI-oxy resulted in no diffraction peak being attributed to mesopores. The presence of large voids in MFI-oxy induced relatively small volumes of micro- and mesopores compared to those of other MFI-meso zeolites.

Even though the shape and size of mesopores remarkably vary with their preparation method, their surfaces consisted of a MFI topology. TEM photos shown in Fig. 5 clearly exhibit the presence of the lattice fringe of MFI zeolite (a) on the MFI-meso zeolites. The Fourier-transformation of the lattice fringes after noise removal using a soft Wiener filter produced electron diffractions (b), indicating the presence of a crystalline zeolite moiety. The difference in the arrangement of the MFI zeolite framework resulted in different lattice fringes of MFI zeolites in terms of spacing and orientation. However, the obtained lattices of MFI zeolite (c) from the electron diffractions were in good accordance with that of MFI zeolite *Pnma* where the lattice parameters were $a = 2.007$ nm, $b = 1.992$ nm, and $c = 13.42$ nm [35]. The simulation of the lattice structure of the MFI zeolite based on the electron diffractions using NCEMSS confirmed the presence of the MFI framework [36]. This suggests that the fundamental framework of the MFI-meso zeolites, regardless of the shape and size of mesopores, is composed of the MFI topology.

A unique property of the zeolite framework is the tetrahedral coordination of aluminum atoms with four oxygen atoms. The ^{27}Al MAS NMR spectra of the MFI-meso zeolites, shown in Fig. S2, confirmed the tetrahedral coordination of aluminum atoms by their peaks at 50 ppm. The absence of the peak at around 0 ppm attributed to octahedral coordination of aluminum atoms suggested most detected aluminum atoms of MFI zeolites had tetrahedral coordination, because the signals attributed to aluminum atoms with octahedral coordination were not observed. The introduction of mesopores into the MFI-meso zeolites did not induce the formation of appreciable alumina moieties with octahedral coordination.

The presence of mesopores affects the acidity of the MFI-meso zeolites. Fig. 6 shows TPD profiles of ammonia that was divided by two desorption peaks with maxima around 250 and 350 °C: the low-temperature and high-temperature peaks are attributed to weak and strong acid sites, respectively [37]. However, the MFI-plate and MFI-nano without mesopores show only large high-temperature peaks, indicating the presence of large amounts of strong acid sites. MFI-alk and MFI-sda have relatively large amounts of both weak and strong acid sites. MFI-syn had a medium amount of strong acid sites, while the amounts of strong acid sites were very small on MFI-oxy. The relative amount of strong acid sites on MFI-meso zeolites, such as MFI-syn, MFI-sda, and MFI-alk, were around 0.4 on MFI-plate. However, the relative amount of strong acid sites on MFI-oxy was 0.05 and demonstrated the extremely small amount of strong acid sites. These results indicate that the introduction of mesopores into the MFI zeolite considerably reduced the amount of strong acid sites and the reduction was significantly severe on MFI-oxy.

The introduction of mesopores into the MFI zeolite significantly enhances the rate of mass transfer. Since the molecular size of *o*-xylene is comparable to the channel size of MFI zeolite, its uptake rate reflects the restriction in mass transfer [10]. Fig. 7 exhibits the uptake curves of *o*-xylene on the MFI-meso zeolite and reference MFI zeolites. The uptake of *o*-xylene onto MFI-plate proceeded very slowly even after 60 min, while that onto MFI-nano with small nano sized particles was rapid and achieved adsorption equilibrium at 30 min. The adsorption equilibriums of *o*-xylene on MFI-sda and MFI-syn were achieved at 10 min, indicating that the introduction of mesopores enhanced the rate of mass transfer and this allowed for the achievement of rapid mass transfer compared to MFI-nano. The formation of mesopores, however, reduced the micropore volumes of MFI-meso zeolites, resulting in the reduction of the uptake amount of *o*-xylene.

Scheme 1 illustrates the characteristics of mesopores that were deduced from characterization results of the MFI-meso zeolites. The mesopores of MFI-syn and MFI-sda were composed of MFI zeolite, and they were highly ordered due to the formation of MFI zeolite on the micelles of sda molecules. Therefore, the amounts of mesopores on them were relatively large, while those of the zeolite moiety were small. Their crystalline MFI framework resulted in the formation of strong acid sites. The alkaline treatment irregularly dissolved zeolite and resulted in the formation of irregular mesopores and the retention of strong acid sites on the remaining zeolitic moiety. The addition of the oxyacid into the synthetic mixture of MFI zeolite produced large voids accompanying small amounts of mesopores and zeolite moieties on MFI-oxy. The small amount of zeolite moieties resulted in the small amount of strong acid sites. The highly crystallized MFI-plate and MFI-nano had large amounts of strong acid sites. The small amount of mesopores on the MFI-nano was responsible for the agglomeration of nano-sized particles.

3.2. Catalytic degradation of PEs with different skeletal structures

PEs are classified into HDPE, LDPE, and LLDPE according to their skeletal structures, but their fundamental constituent is the same, and that is the C–C bond. Therefore, the conversion profiles of PEs with respect to thermal degradation, regardless of their skeletal structure, are highly coincident, as shown in Fig. S3, because thermal degradation is proceeds through radicals produced from the fission of C–C bonds [38]. The thermal degradation of PEs was negligible at 350 °C and the conversions were less than 5%,

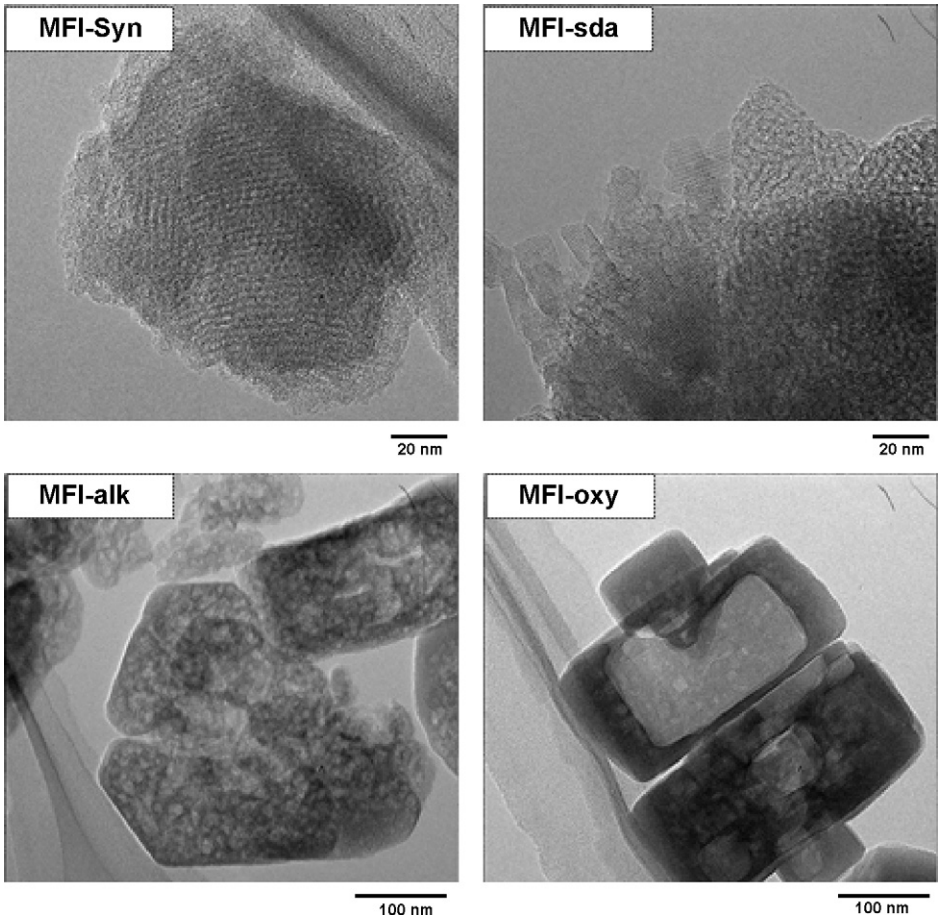

Fig. 4. TEM images of MFI-meso zeolites.

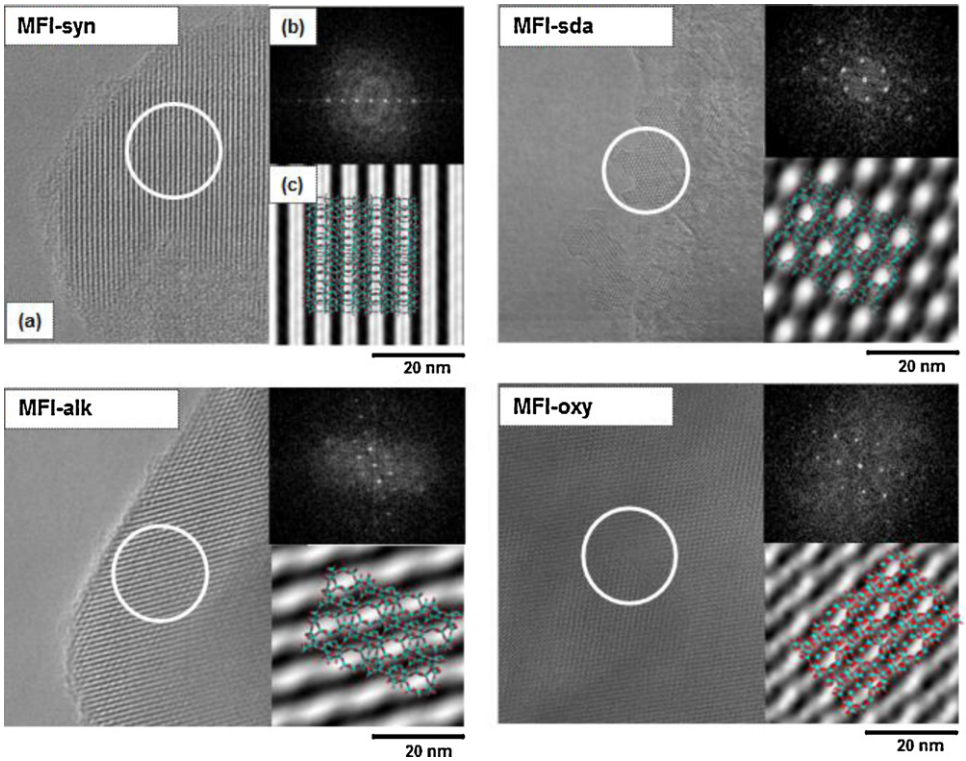

Fig. 5. TEM images of MFI-meso zeolites: (a) lattice fringe, (b) electron diffraction, and (c) simulated lattice structure of MFI framework.

Table 1
Compositions and porous properties of the MFI zeolites.

Catalyst	Si/Al ratio		Pore volume (cm^3/g)			S_{BET} (m^2/g)	Particle size (μm)	Relative amount of strong acid sites
	ICP	EDX	Micropore	Mesopore	Total			
MFI-syn	33	32	0.21	0.66	0.82	681	–	0.28
MFI-sda	15	12	0.15	0.45	0.60	467	0.5	0.44
MFI-alk	14	14	0.13	0.39	0.52	336	0.2–0.4	0.46
MFI-oxy	14	14	0.11	0.13	0.24	281	0.3	0.05
MFI-nano	35	33	0.16	0.22	0.38	431	0.2	0.95
MFI-plate	23	19	0.14	0.06	0.20	335	2.0	1.00

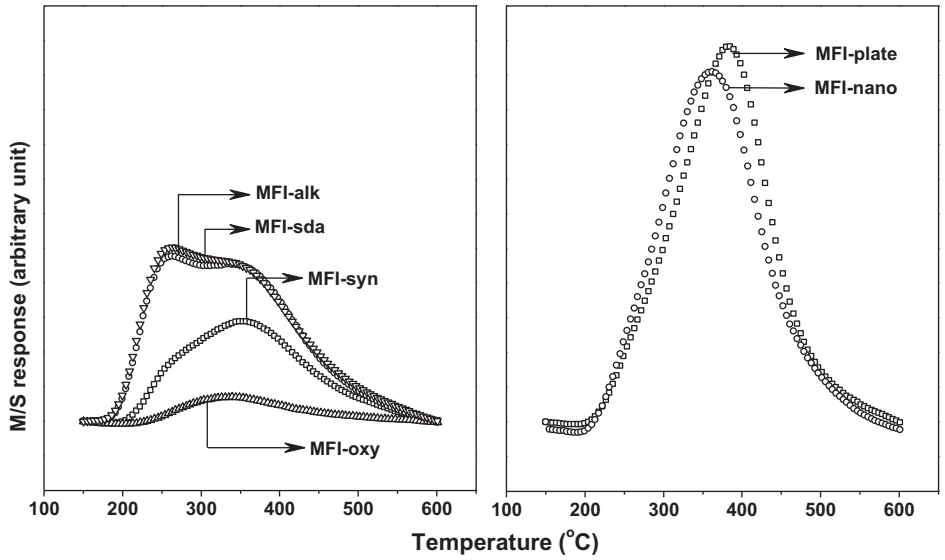

Fig. 6. TPD profiles of ammonia from MFI zeolites.

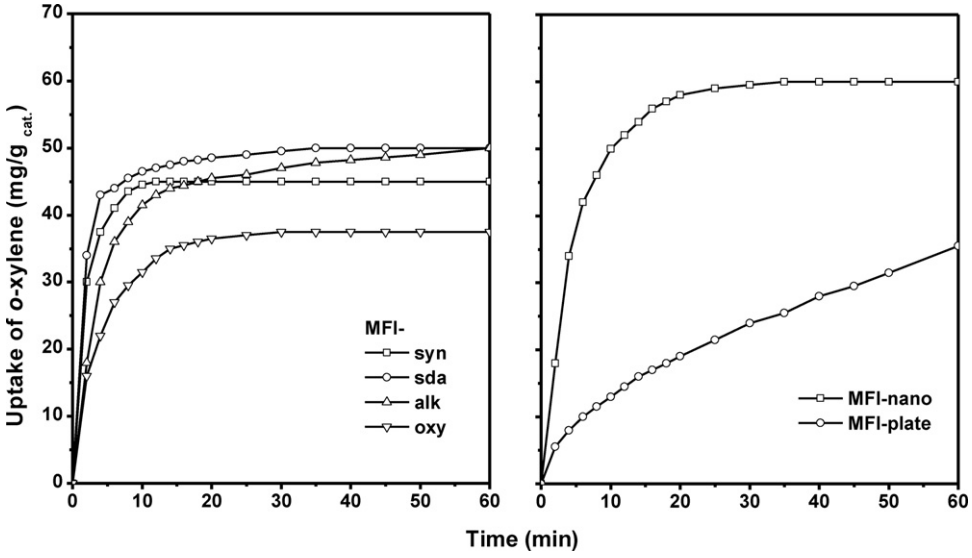

Fig. 7. Uptake curves of *o*-xylene on MFI zeolites at 120 °C.

even at 380 °C. The conversion increased rapidly with increasing temperatures above 400 °C and a conversion of 80% was achieved at 450 °C. Therefore, the catalytic degradation was investigated at 380 °C to minimize the contribution of thermal degradation. Table S1 lists the yields of liquid and gas products accompanying the conversion in the catalytic degradation. The sums of gas and liquid products yields determined by the collection of products were coincident with the conversion determined from the loss of reactant which ranged from 1 to 8%, indicating that the examination method of the degradation was reasonable.

The introduction of mesopores into MFI zeolites significantly influences their catalytic activity in the liquid-phase degradation of PEs. Fig. 8 shows the conversion profiles of HDPE on the MFI-meso zeolites along with temperature. The catalyst loading was reduced to 0.05 g/20 g of HDPE to maximize the difference in the conversion according to the catalysts. The degradation of HDPE

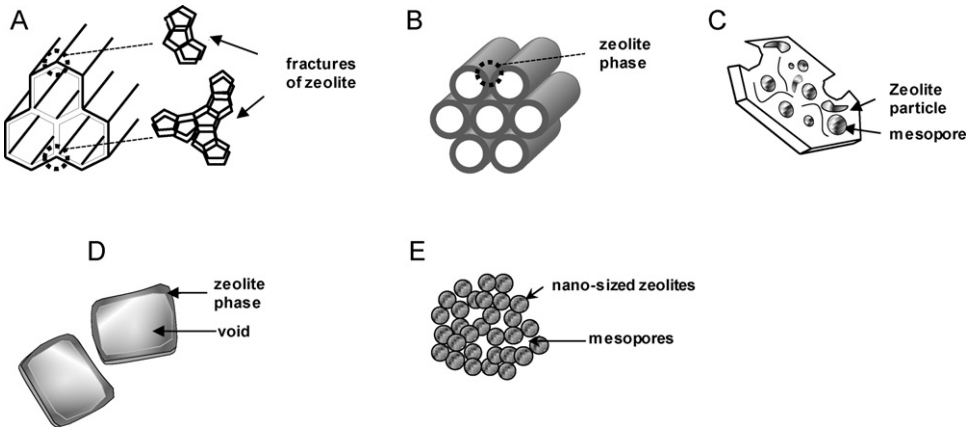

Scheme 1. Schematic shapes of mesopores on MFI-meso zeolites; (A) MFI-syn, (B) MFI-sda, (C) MFI-alk, (D) MFI-oxy, and (E) MFI-nano.

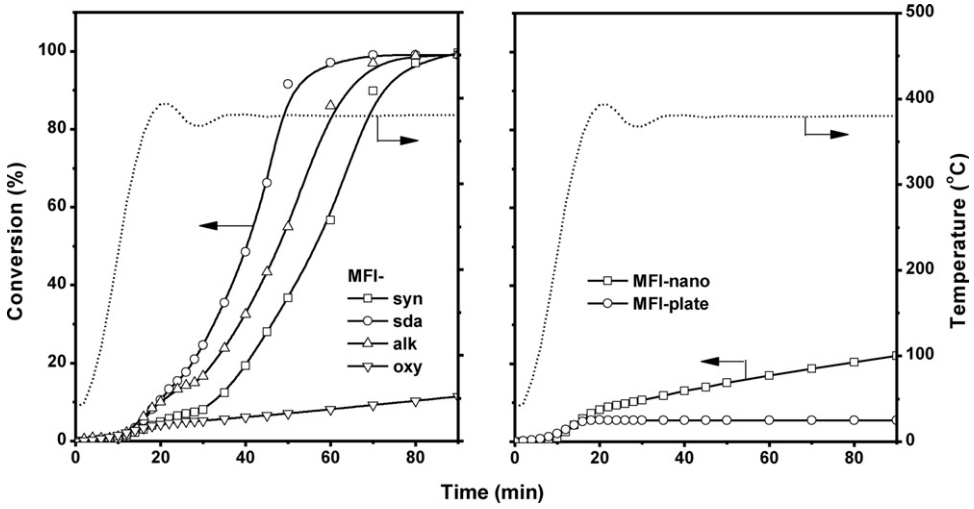

Fig. 8. Conversion profiles over MFI zeolites in the degradation of HDPE. HDPE/MFI = 20 g/0.05 g at 380 °C.

was very rapid on MFI-sda, MFI-alk, and MFI-syn and 100% conversion was achieved at 60 min, while the degradation on MFI-oxy was slow, indicating that the characteristics of mesopores were important in determining catalytic activity. Almost no catalytic activity was observed on MFI-plate. The considerably low conversion on MFI-nano, even with nano-sized small particles under the same conditions, clearly differed from the exceptional activity of the MFI-meso zeolites. The large particles of MFI-plate resulted in a negligible conversion, and the low conversion on MFI-oxy was responsible for its small amount of strong acid sites. Nevertheless, the complete conversion of HDPE on MFI-sda, MFI-alk, and MFI-syn suggested the powerful contribution of mesopores with respect to the degradation of HDPE.

Contrary to the conversion profiles, the distribution of carbon number in the liquid products of the HDPE degradation, shown in Fig. S4, were almost the same, regardless of acidity and the presence of mesopores. The HDPE loading was reduced to 10 g/0.05 g of catalysts to obtain reasonable levels of conversions. The yields of C_5 hydrocarbon were the highest among hydrocarbons on all the MFI zeolites and the yield of hydrocarbons decreased as their carbon number increased. In the gas products, propylene exhibited the highest yield. The same product distributions of the liquid and gas products on the MFI zeolites indicated that the degradation of HDPE proceeded through the same degradation mechanism, although their catalytic activity varied widely according to the acidic and porous characteristics.

The skeletal structure of PEs also influences their catalytic degradation, as shown in Fig. 9. In the degradation of HDPE, MFI-oxy exhibited a relatively low conversion profile compared to other MFI-meso zeolites. A slight high conversion profile over MFI-alk was comparable to that over MFI-sda, contrary to the degradation result of HDPE with 20 g/0.05 g of catalysts (Fig. 8), and this might be due to the slightly high number of strong acid sites of the former compared to that of the latter. In the degradation with a low loading of catalysts, the deactivation by coke deposition in mesopores lowered the conversion of HDPE over MFI-alk because of its small mesopore volume which induced rapid deactivation [32]. On the contrary, four MFI-meso zeolites exhibited similar conversion profiles in the degradation of LDPE, while MFI-oxy illustrated very low activity in the degradation of LLDPE. The reactivity of PEs in the degradation over the MFI-meso zeolites, except for MFI-oxy, increased in the order of LLDPE < LDPE < HDPE, while that on MFI-meso-oxy increased in the order of LLDPE $\ll$ LDPE $\approx$ HDPE.

The slow degradation of LDPE on the MFI-meso zeolites was due to the diffusion limitation of LDPE with its large branched hydrocarbons with bulky structures, but the easy formation of tertiary carbenium ions from LDPE minimized the difference in their conversions according to the pore structure and acidic properties of catalysts [39]. Therefore, MFI-oxy with the smallest number of strong acid sites exhibited a similar conversion profile to other MFI-meso zeolites. Although LLDPE also has branched chains like LDPE, its branched chains are rare and relatively short (like C_2 and C_4).

Table 2
Physico-chemical and catalytic activities of MFI zeolites in the degradation of PEs.

MFI zeolite	Physico-chemical property		Catalytic activity (as $t_{50\%}$, min)			
	Mesopore volume (cm^3/g)	Relative amount of strong acid sites	HDPE		LDPE	LLDPE
			20 g/0.05 g[a]	10 g/0.05 g	10 g/0.05 g	10 g/0.05 g
MFI-plate	0.06	1.00	–	–	26	–
MFI-nano	0.22	0.95	–	21	30	50
MFI-oxy	0.13	0.05	–	29	24	–
MFI-syn	0.66	0.28	56	18	20	38
MFI-sda	0.45	0.44	41	19	20	32
MFI-alk	0.39	0.46	48	16	20	32

'–' indicates non-measurable $t_{50\%}$ within 60 min.
[a] PE/catalyst loading ratio (as mass).

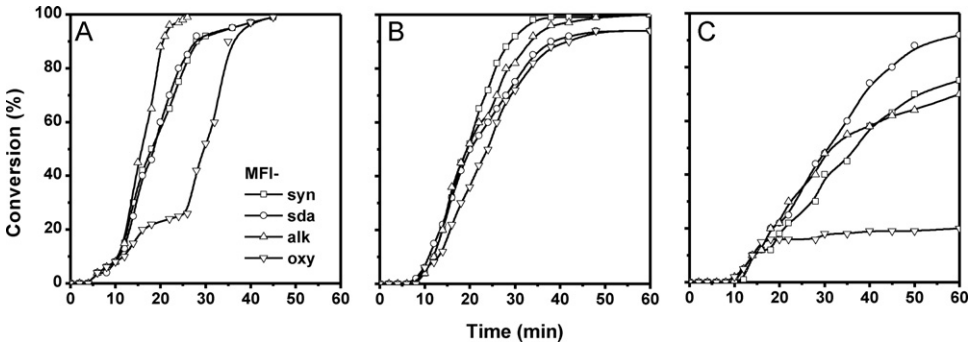

Fig. 9. Conversion profiles over MFI-meso zeolites in the degradation of PEs with different structures at 380 °C. (A) HDPE, (B) LDPE, and (C) LLDPE. PE/MFI = 10 g/0.05 g.

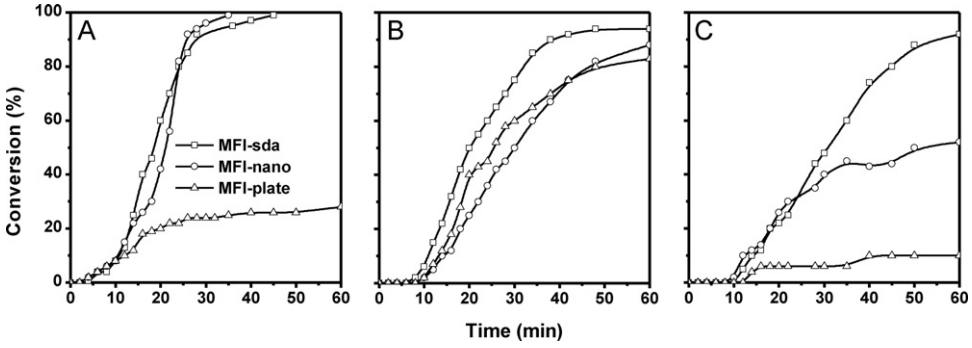

Fig. 10. Conversion profiles over MFI zeolites in the degradation of PEs with different structures at 380 °C. (A) HDPE, (B) LDPE, and (C) LLDPE. PE/MFI = 10 g/0.05 g.

The main linear hydrocarbons of LLDPE lowered the feasibility of forming tertiary carbenium ions. The slow degradation of LLDPE compared to those of HDPE and LDPE even on the MFI-meso zeolites was rational because both strong acid sites and mesopores were simultaneously required. MFI-oxy with the smallest number of strong acid sites had the lowest conversion profile for LLDPE, about 20% at 20 min, due to its weak acidity and the small mesopore volume.

The conversion profiles of HDPE, LDPE, and LLDPE on MFI-sda, MFI-nano, and MFI-plate are compared in Fig. 10 to clearly discuss the role of mesopores, the contribution of external surface area, and the effect of acidity on the liquid-phase degradation of PEs. MFI-sda had many regularly ordered mesopores with a high external surface area and high number of strong acid sites, while MFI-nano had a high number of strong acid sites and a large external surface due to its small particles. MFI-plate had a high number of strong acid sites, but it had negligible external surface area and no mesopores. In the degradation of HDPE, the significant contribution of the external surface resulted in high conversions on MFI-sda and MFI-nano, while MFI-plate with a negligible external surface exhibited very low conversions. The easy formation of carbenium ions during the degradation of LDPE on the external surface and the slow diffusion of reactants and products in the micropores of MFI zeolites minimized the difference in the conversion profiles on the zeolites. However, the difference in the conversion profiles were magnified during the degradation of LLDPE that had rare short branched chains on its skeleton. The degradation of LLDPE was slow on MFI-sda, MFI-nano, and MFI-plate compared to those of HDPE and LDPE. Furthermore, the MFI-plate with a negligible external surface exhibited about 10% conversion, indicating the importance of the external surface for the primary initiation of the degradation.

Table 2 lists the physico-chemical properties and catalytic activities of MFI zeolites. The catalytic activities were represented by the time required for 50% conversion, $t_{50\%}$. A small value of $t_{50\%}$ indicated high catalytic activity. In the degradation of HDPE at 20 g of HDPE/0.05 g catalyst, MFI-alk, MFI-sda and MFI-syn exhibited high catalytic activity, whereas $t_{50\%}$ were too long to measure over MFI-plate, MFI-nano and MFI-oxy indicating low catalytic activities. The former have both high numbers of strong acid sites and high mesopore volumes, whereas the latter have not. The increase in the catalyst loading by lowering PE loading per constant weight of catalyst considerably shortened $t_{50\%}$. The MFI-syn, -sda and -alk

still exhibited high activities compared to MFI-plate, -nano and -oxy. The smallest external surface of MFI-plate was responsible for its lowest activity even at 10 g of HDPE/0.05 g catalyst. The large external surface of MFI-nano and MFI-oxy caused the shortened $t_{50\%}$. The slightly high activity of MFI-alk compared to that of MFI-sda might be due to the high number of strong acid sites. Since mesopores do not suppress the formation of large molecules, the precursor of coke deposit in mesopore unlike sinusoidal micropores of MFI zeolite induces severe deactivation. The small volume of mesopores on MFI-alk was rapidly blocked by coke, resulting in a low conversion when the catalyst loading was small compared to HDPE loading, but the contribution of strong acid sites became more significant when the catalyst loading was high.

The MFI zeolites exhibited considerably different catalytic activities in the degradation of LDPE compared to that of HDPE due to its different chain structures. The $t_{50\%}$ of LDPE was in a narrow range of 20–30 min, regardless of acidity and mesopore volume of the MFI zeolites. The catalytic degradation of PE usually proceeded through two steps: the first degradation over the acid sites on the external surface producing carbenium ions and the second degradation at the entrances of pores and in the micropores, producing fragmented final products. The easy formation of tertiary carbenium ions reduces the contribution of acidity and mesopores, resulting in the rapid degradation of LDPE even over MFI-plate, -nano and -oxy. The relatively low activity of MFI-nano compared to MFI-plate might be corresponded to that the former had a slightly small number of strong acid sites, but more understanding on the degradation is required for more plausible explanation.

The $t_{50\%}$ over the MFI zeolites in the degradation of LLDPE exhibited a very similar trend to those in the degradation of HDPE, except the long $t_{50\%}$ values. The short branched chains of LLDPE on its skeleton suppress the close contact of LLDPE to acid sites, resulting in a low conversion. The small external surface area of MFI-plate and the smallest amount of strong acid sites of MFI-oxy were responsible for their low activities. The rapid mass transfer through the mesopores of MFI-alk, -sda and -syn caused the relatively rapid degradation of LLDPE compared to MFI-nano. The mesopores directly connected to micropores on the MFI-meso zeolites exhibited higher activity than MFI-nano with mesopores composed among aggregated nano-sized particles.

In summary, both the high number of strong acid sites and the presence of mesopores directly connected to micropores are important factors in determining the activity of MFI zeolites in the degradation of PEs. In the degradation of HDPE over the MFI zeolites, the high number of strong acid sites and the presence of mesopores are essential for high activity. On the contrary, the easy formation of tertiary carbenium ions from LDPE minimized the contribution of strong acid sites and mesopores to its degradation, resulting in similar activities of MFI zeolites. The activity of MFI zeolites in the degradation of LLDPE exhibited a similar trend to that in the degradation of HDPE, except their low activities due to the slow mass transfer of reactants and products.

The quantitative comparison of the activity in the liquid-phase degradation of PEs on zeolite catalysts is very difficult because the degradation conditions, such as a catalyst loading to PE, temperature, and reactor type, were largely different. The complete conversions of HDPE and LDPE was obtained at 430 °C when the mass ratio of PE to the catalyst was 100 [6,14,16]. Therefore, the high conversion (>95) of HDPE, LDPE, and LLDPE on MFI-sda, MFI-syn, and MFI-alk at 380 °C when the mass ratio of PE to the catalyst was 400 suggested a significant contribution of mesopores to the catalytic degradation of PEs by increasing the external surface area for the initial degradation and by enhancing mass transfer through mesopores.

4. Conclusions

1. The shape and size of mesopores developed on the MFI-meso zeolites were largely dependent on their preparation method, but the surfaces of the mesopores were consistently composed of the MFI framework.
2. The MFI-syn zeolite was synthesized from the synthetic mixture containing MFI fragments dissolved in an alkali solution and the MFI-sda zeolite was prepared by using OTAC as a sda. These MFI-meso zeolites exhibited highly ordered mesopores, but the MFI-alk zeolite that was prepared by treatment with an alkaline solution produced irregular sphere type mesopores. The addition of an oxyacid into the synthetic mixture caused the formation of large voids accompanying small amounts of zeolitic phase and mesopores.
3. The amounts of strong acid sites on MFI-sda, MFI-syn, and MFI-alk were smaller than highly crystalline MFI-plate and MFI-nano, but they were relatively larger than MFI-oxy.
4. MFI-sda, MFI-syn, and MFI-alk with large numbers of strong acid sites and suitable amounts of mesopores exhibited exceptional activities in the liquid-phase degradation of PEs even compared to MFI-nano with nano-sized small particles, indicating the effectiveness of mesopores in degradation. The introduction of mesopores into the MFI zeolite with strong acid sites significantly enhanced its catalytic activity in the degradation of HDPE and LLDPE because the initial degradation on the external surface was important in determining the degradation rate, while the enhancement of the catalytic activity by the introduction of mesopore was not considerable in the degradation of LDPE because of the easy formation of carbenium ions from LDPE on the external surface.

Acknowledgements

This work was supported by the Priority Research Centers Program through the National Research Foundation of Korea (NRF) funded by the Ministry of Education, Science and Technology (2010-0029626).

Appendix A. Supplementary data

Supplementary data associated with this article can be found, in the online version, at doi:10.1016/j.apcatb.2011.08.009.

References

[1] R. Bagri, P.T. Williams, J. Anal. Appl. Pyrolysis 62 (2002) 29–41.
[2] M.R. Hernández, Á.N. García, A. Marcilla, J. Anal. Appl. Pyrolysis 78 (2007) 272–281.
[3] I.C. Neves, G. Botelho, A.V. Machado, P. Rebelo, S. Ramôa, M.F.R. Pereira, A. Ramanathan, P. Pescarmona, Polym. Degrad. Stab. 92 (2007) 1513–1519.
[4] J. Aguado, D.P. Serrano, G.S. Miguel, J.M. Escola, J.M. Rodríguez, J. Anal. Appl. Pyrolysis 78 (2007) 153–161.
[5] P. Gaca, M. Drzewiecka, W. Kaleta, H. Kozubek, K. Nowińska, Pol. J. Environ. Stud. 17 (2008) 25–31.
[6] S.J. Choi, Y.-K. Park, K.-E. Jeong, T.-W. Kim, H.-J. Chae, S.H. Park, J.-K. Jeon, S.-S. Kim, Korean J. Chem. Eng. 27 (5) (2010) 1446–1451.
[7] Y.S. González, C. Costa, M.C. Márquez, P. Ramos, J. Hazard. Mater. 187 (2011) 101–112.
[8] J. Agullo, N. Kumar, D. Berenguer, D. Kubicka, A. Marcilla, A. Gómez, T. Salmi, D.Y. Murzin, Kinet. Catal. 48 (2007) 570–575.
[9] Y.J. Lee, J.-H. Kim, S.H. Kim, S.B. Hong, G. Seo, Appl. Catal. B-Environ. 83 (2008) 160–167.
[10] Y.S. You, J.-H. Kim, G. Seo, Polym. Degrad. Stab. 70 (2000) 365–371.
[11] D.P. Serrano, J. Aguado, J.M. Rodríguez, A. Peral, J. Anal. Appl. Pyrolysis 79 (2007) 456–464.
[12] C. Covarrubias, F. Gracia, H. Palza, Appl. Catal. A-Gen. 384 (2010) 186–191.
[13] J.F. Mastral, C. Berrueco, M. Gea, J. Ceamanos, Polym. Degrad. Stab. 91 (2006) 3330–3338.
[14] D.P. Serrano, J. Aguado, J.M. Escola, J.M. Rodríguez, J. Anal. Appl. Pyrolysis 74 (2005) 353–360.

[15] Y.-H. Lin, M.-H. Yang, T.-F. Yeh, M.-D. Ger, Polym. Degrad. Stab. 86 (2004) 121–128.
[16] R.A. García, D.P. Serrano, D. Otero, J. Anal. Appl. Pyrolysis 74 (2005) 379–386.
[17] L.B. Pierella, S. Renzini, O.A. Anunziata, Microporous Mesoporous Mater. 81 (2005) 155–159.
[18] A. Petushkov, S. Yoon, S.C. Larsen, Microporous Mesoporous Mater. 137 (2011) 92–100.
[19] X. Zhu, L.L. Lobban, R.G. Mallinson, D.E. Resasco, J. Catal. 271 (2010) 88–98.
[20] A.N.C. Van Laak, L. Zhang, A.N. Parvulescu, P.C.A. Bruijincx, B.M. Weckhuysen, K.P. de Jong, P.E. de Jongh, Catal. Today 168 (2011) 48–56.
[21] Y. Tao, H. Kanoh, K. Kaneko, Adsorption 12 (2006) 309–316.
[22] Y. Tao, H. Kanoh, L. Abrams, K. Kaneko, Chem. Rev. 106 (2006) 896–910.
[23] S. Inagaki, M. Ogura, T. Inami, Y. Sasaki, E. Kikuchi, M. Matsukata, Microporous Mesoporous Mater. 74 (1998) 163–170.
[24] M.K. Choi, H.S. Cho, R. Srivastava, C. Venkatesan, D.-H. Choi, R. Ryoo, Nat. Mater. 5 (2006) 718–723.
[25] R. Kumar, P. Mukherjee, R.K. Pandey, P. Rajmohanan, A. Bhaumik, Microporous Mesoporous Mater. 22 (1998) 23–31.
[26] Y.H. Chou, C.S. Cundy, A.A. Garforth, V.L. Zholobenko, Microporous Mesoporous Mater. 89 (2006) 78–87.
[27] A. Coelho, I.M. Fonseca, I. Matos, M.M. Marques, A.M.M. do Rego, M.A.N.D.A. Lemos, Appl. Catal. A-Gen. 374 (2010) 170–179.
[28] A. Marcilla, A. Gómez-Siurana, F. Valdés, J. Anal. Appl. Pyrolysis 79 (2007) 433–442.
[29] A. Marcilla, M.I. Beltrán, R. Navarro, Appl. Catal. A-Gen. 333 (2007) 57–66.
[30] E.F.B. Silva, M.P. Ribeiro, L.P.F.C. Galvão, V.J. Fernandes, A.S. Araujo, J. Therm. Anal. Calorim. 103 (2011) 465–469.
[31] S. Sarathy, M.D. Wallis, S.K. Bhatia, Chem. Eng. Sci. 65 (2010) 796–806.
[32] D.H. Choi, J.W. Park, J.-H. Kim, Y. Sugi, G. Seo, Polym. Degrad. Stab. 91 (2006) 2860–2866.
[33] N. Erdman, O. Warschkow, M. Asta, K.R. Poeppelmeier, D.E. Ellis, L.D. Marks, J. Am. Chem. Soc. 125 (2003) 10050–10056.
[34] C. Baerlocher, W.M. Meier, D.H.E. Olson, Atlas of Zeolite Framework Types, 5th ed., Elsevier, Amsterdam, 2001.
[35] M.A. O'Keefe, R. Kilaas, Scanning Microscopy Supplement 2 (1988) 225–244.
[36] J.J. Hu, F.H. Li, H.F. Fan, Ultramicroscopy 41 (1992) 387–397.
[37] N. Katada, H. Igi, J.-H. Kim, M. Niwa, J. Phys. Chem. B 101 (1997) 5969–5977.
[38] H. Bockhorn, A. Hornung, U. Hornung, J. Anal. Appl. Pyrolysis 50 (1999) 77–101.
[39] A.J. Peacock, Handbook of Polyethylene, Marcel Dekker, Inc., New York, 2000.